

Molecular Drug Imaging: ^{89}Zr -Bevacizumab PET in Children with Diffuse Intrinsic Pontine Glioma

Marc H. Jansen*¹, Sophie E.M. Veldhuijzen van Zanten*¹, Dannis G. van Vuurden¹, Marc C. Huisman², Danielle J. Vugts², Otto S. Hoekstra², Guus A. van Dongen², and Gert-Jan L. Kaspers¹

¹*Pediatric Oncology/Hematology, Department of Pediatrics, VU University Medical Center, Amsterdam, The Netherlands; and*

²*Department of Radiology and Nuclear Medicine, VU University Medical Center, Amsterdam, The Netherlands*

Predictive tools for guiding therapy in children with brain tumors are urgently needed. In this first molecular drug imaging study in children, we investigated whether bevacizumab can reach tumors in children with diffuse intrinsic pontine glioma (DIPG) by measuring the tumor uptake of ^{89}Zr -labeled bevacizumab by PET. In addition, we evaluated the safety of the procedure in children and determined the optimal time for imaging. **Methods:** Patients received ^{89}Zr -bevacizumab (0.1 mg/kg; 0.9 MBq/kg) at least 2 wk after completing radiotherapy. Whole-body PET/CT scans were obtained 1, 72, and 144 h after injection. All patients underwent contrast (gadolinium)-enhanced MRI. The biodistribution of ^{89}Zr -bevacizumab was quantified as SUVs. **Results:** Seven DIPG patients (4 boys; 6–17 y old) were scanned without anesthesia. No adverse events occurred. Five of 7 primary tumors showed focal ^{89}Zr -bevacizumab uptake (SUVs at 144 h after injection were 1.0–6.7), whereas no significant uptake was seen in the healthy brain. In 1 patient, multiple metastases all showed positive PET results. We observed inter- and intratumoral heterogeneity of uptake, and ^{89}Zr -bevacizumab uptake was present predominantly (in 4/5 patients) within MRI contrast-enhanced areas, although ^{89}Zr -bevacizumab uptake in these areas was variable. Tumor targeting results were quantitatively similar at 72 and 144 h after injection, but tumor-to-blood-pool SUV ratios increased with time after injection ($P = 0.045$). The mean effective dose per patient was 0.9 mSv/MBq (SD, 0.3 mSv/MBq). **Conclusion:** ^{89}Zr -bevacizumab PET studies are feasible in children with DIPG. The data suggest considerable heterogeneity in drug delivery among patients and within DIPG tumors and a positive, but not 1:1, correlation between MRI contrast enhancement and ^{89}Zr -bevacizumab uptake. The optimal time for scanning is 144 h after injection. Tumor ^{89}Zr -bevacizumab accumulation assessed by PET scanning may help in the selection of patients with the greatest chance of benefit from bevacizumab treatment.

Key Words: brain stem neoplasm; PET; ^{89}Zr -bevacizumab; pharmacokinetics

J Nucl Med 2017; 58:711–716

DOI: 10.2967/jnumed.116.180216

The need for predictors to guide therapy in individual patients applies to the entire field of pediatric oncology but, in particular,

Received Jul. 14, 2016; revision accepted Sep. 20, 2016.

For correspondence or reprints contact: Guus A. van Dongen, Department of Radiology and Nuclear Medicine, VU University Medical Center, De Boelelaan 1118, 1081 HV Amsterdam, The Netherlands.

E-mail: gams.vandongen@vumc.nl

*Contributed equally to this work.

Published online Oct. 20, 2016.

COPYRIGHT © 2017 by the Society of Nuclear Medicine and Molecular Imaging.

to malignant brain tumors. One of the most challenging brain tumors in children is diffuse intrinsic pontine glioma (DIPG), a lethal childhood malignancy of the brain stem comprising 10% of all pediatric central nervous system tumors (1). DIPG tumors are resistant to all kinds of systemic therapies, including targeted agents, and hardly any patient survives beyond 2 y from diagnosis (2,3). One hypothesis for therapy failure is that drugs actually do not reach the tumors, as in most DIPG tumors at diagnosis MRI shows little or no gadolinium contrast enhancement, suggesting an intact blood-brain barrier for large molecules (4). Molecular drug imaging may help in the investigation of this hypothesis; however, despite a recent boost in molecular drug imaging in adults, no immuno-PET imaging studies have yet been performed in children (5).

Recent messenger RNA profiling studies revealed overexpression of the proangiogenic vascular endothelial growth factor (VEGF) in DIPG compared with the normal brain and compared with adult high-grade glioma, a result that makes proangiogenic VEGF a potential drug target (6,7). The biologic activity of VEGF can be neutralized by bevacizumab, a recombinant humanized monoclonal antibody. The potential of bevacizumab in DIPG is being studied in several trials (clinicaltrials.gov: NCT01182350; Trialregister.nl: NTR2391), but few trials have been published (8–10). The overall survival outcome in these DIPG trials was as poor as in patients receiving standard treatment (8,9), but individual patients with significant responses and prolonged survival after bevacizumab treatment have been reported (10,11). Hence, the challenge is to identify patients who will benefit from bevacizumab treatment.

^{89}Zr -labeled bevacizumab PET imaging may help in assessment of the inter- and inpatient heterogeneity of drug biodistribution in vivo, thereby predicting the presence or absence of a response in patients subsequently treated with bevacizumab. Studies in both mice and adult patients confirmed that ^{89}Zr -bevacizumab PET imaging was feasible and able to reveal bevacizumab accumulation in VEGF-positive tumors (7,12–14). In addition, in adult renal cancer tumors, ^{89}Zr -bevacizumab uptake was correlated with a response to bevacizumab treatment (13). The results of our preclinical research with ^{89}Zr -bevacizumab in mice suggested poor bevacizumab uptake in intracranial tumors; using pontine, striatal, and subcutaneous glioma mouse models, we found no significant uptake of ^{89}Zr -bevacizumab in intracranial tumors at any stage of the disease or in the normal nonneoplastic surrounding brain in any of the tumor models used (7). In contrast, a high level of accumulation of ^{89}Zr -bevacizumab was observed in the subcutaneous glioma xenograft. Therefore, poor bevacizumab distribution in the brain seemed to be a major issue, but we also observed a significantly lower level of VEGF expression in intracranial tumors than in the subcutaneous glioma xenograft.

As a first step in investigating the clinical utility of immuno-PET in this setting, we performed a pilot study to investigate whether bevacizumab can reach tumors in children with DIPGs by measuring the tumor uptake of ^{89}Zr -bevacizumab. In addition, we assessed the optimal time for PET imaging, evaluated the biodistribution and radiation dosimetry of ^{89}Zr -bevacizumab, and ascertained the safety and tolerability of scanning procedures without anesthesia.

MATERIALS AND METHODS

Study Population

The study was conducted at VU University Medical Center, Amsterdam, The Netherlands. DIPG patients who were 4–18 y old and had completed radiotherapy (the standard DIPG therapy) at least 2 wk earlier were eligible. Patients with a known hypersensitivity to humanized monoclonal antibodies were excluded, as were those previously treated with bevacizumab or any other anti-VEGF agent. To reduce patient burden, PET-related blood sampling and the use of anesthetics were not allowed. The latter was the reason for the minimum age of 4 y, as children younger than 4 y were not expected to complete a PET scan with no movement artifacts without the use of anesthesia.

For all subjects, both parents signed a written informed consent form. In addition, all subjects who were at least 12 y old signed a written informed consent form. The study (registered as NTR3518 in The Netherlands National Trial Register) was approved by the Dutch Central Committee on Research Involving Human Subjects and the Institutional Review Board of VU University Medical Center and was performed in accordance with the Declaration of Helsinki.

To determine the optimal time for scanning (72 or 144 h after injection), we aimed to include at least 5 patients with visible tumor uptake of ^{89}Zr -bevacizumab. These postinjection times were based on previous research in mice and clinical studies in adults with ^{89}Zr -bevacizumab (7,12,14).

^{89}Zr -Bevacizumab Labeling, Infusion, and PET Procedures

The production and purification of ^{89}Zr and its coupling to bevacizumab were performed in accordance with good manufacturing practice at VU University Medical Center. The labeling process as well as quality controls were described previously (15–17), and the results were similar to those described by Bahce et al. (14). The administered dose of ^{89}Zr -bevacizumab (0.1 mg/kg; 0.9 MBq/kg) was 1% of the therapeutic bevacizumab dose in humans.

Patients were imaged with a whole-body Philips Gemini TF64 PET/CT scanner (18). Each PET scan was preceded by a low-dose CT scan with routinely applied settings. The CT scan was followed by a 10-min static PET/CT scan covering the brain and a whole-body PET scan (4 min per bed position covering the neck to the upper legs and 1 min covering the legs). PET scans were performed at 1, 72, and 144 h after injection. Patients were clinically observed for 3 h after injection to check for allergic reactions, and they were instructed to contact the hospital in case of later adverse events. All patients underwent T1-weighted pre- and postgadolinium MRI and T2-weighted MRI without anesthesia (Siemens Sonata 1.5-T MRI scanner) within a 2-wk period before PET.

Image Analysis

Visual analysis of the PET scans was first performed without knowledge of the MRI results. Focal uptake exceeding the local background was considered to be a positive result. Volumes of interest were generated manually for tumors and metastases with enhanced tracer uptake and for the blood pool (1.6 mL in the aortic arch), liver, kidneys, spleen, lungs, and bone (vertebrae). SUVs were calculated as the decay-corrected activity concentration (kBq/mL) per injected dose

(MBq) per body weight (kg). PET images of the brain were coregistered with gadolinium-enhanced T1-weighted MR images to enable comparison of postcontrast MR images with PET images. T2-weighted MRI was used to determine whether ^{89}Zr -bevacizumab uptake was present in the whole tumor or focally. Whole-body dosimetry was performed with OLINDA software (19). This dosimetry model takes into account an age-dependent weight factor.

Statistics

Statistical analyses were performed with SPSS version 19 (IBM SPSS). For correlations between SUV_{mean} ratios and time after injection, a nonparametric correlation test (Kendall τ_b) was used.

RESULTS

Population: Safety and Feasibility

We included 7 patients with primary DIPG tumors; 1 patient had metastatic disease in the spinal cord and subependymal space, and another had tumor extension in the facial nerve. The baseline characteristics of the patients are shown in Table 1. The median age was 8 y (range, 6–17 y), and all patients had been pretreated with radiotherapy (in combination with gemcitabine for 3 patients and in combination with temozolomide for 1 patient). No adverse events were observed after injection of ^{89}Zr -bevacizumab, and all patients tolerated the scans and related procedures well. The duration of the whole-body PET scans (including the brain) ranged from 40 to 50 min. All PET and MR images were of good quality and had no movement artifacts.

^{89}Zr -Bevacizumab Uptake in DIPG

The PET scans of 5 patients showed focally enhanced ^{89}Zr -bevacizumab accumulation in their primary DIPG tumors (tumor transverse size range on MRI, 25–37 mm), whereas the PET scans for 2 patients did not show ^{89}Zr -bevacizumab accumulation (tumor transverse size range on MRI, 36–39 mm) (Figs. 1C and 1E). The results of all tumor PET scans were negative at 1 h after injection and became positive as of 72 h after injection (Fig. 2A). In none of the patients was ^{89}Zr -bevacizumab uptake present throughout the entire tumor, as depicted by T2-weighted MRI. For example, in the T2-weighted image (Fig. 1B), ^{89}Zr -bevacizumab uptake was concentrated on the lower right side of the tumor, but the tumor extended into the whole pons. There was no visually detectable ^{89}Zr -bevacizumab uptake in healthy brain tissue in any patient.

Tumor uptake of the tracer among patients was heterogeneous, with tumor SUVs ranging from 1.0 to 5.3 and from 1.0 to 6.7 at 72 and 144 h after injection, respectively (Fig. 2B). Five DIPG tumors showed focal areas of modest to strong contrast enhancement on gadolinium-enhanced T1-weighted MRI (Fig. 1). Coregistration of PET/MR images revealed focal ^{89}Zr -bevacizumab uptake in these contrast-enhanced areas in 4 of 5 DIPG tumors. For 1 tumor with an area of gadolinium contrast enhancement (transverse enhancement size, 13 mm), the PET results were negative (Fig. 1C). In 1 DIPG tumor, the area of ^{89}Zr -bevacizumab uptake on PET was not in an area of gadolinium contrast enhancement (Fig. 1D). SUVs in gadolinium-positive tumors varied widely (Table 1).

In 1 DIPG patient, 11 metastases were observed, and the PET results for all of them were positive (Fig. 3). The 2 largest metastases were in the spinal cord at the C1 level and in the subependymal space (volumes of 2.0 and 1.2 mL, respectively); the SUV_{mean} s for these metastases were 2.4 and 6.5 at 72 h after injection and 2.5

TABLE 1
Baseline Characteristics and Scanning Results

Patient	Sex	Age (y)	Weight (kg)	Metastases or tumor extension	Treatment before PET study	⁸⁹ Zr dose (MBq)	Adverse events	Tumor transverse diameter (mm)	Gadolinium contrast enhancement on MRI	Tumor uptake of ⁸⁹ Zr-bevacizumab	Tumor SUV 72 h after injection	Tumor SUV 144 h after injection
1	F	6	33	None	RT	30.7	None	25	Small nodular	Yes	1.0	1.0
2	F	17	55	None	RT and gemcitabine	37.1	None	37	Ring	Yes	5.3	6.7
3	M	7	28	None	RT	24.2	None	36	Ring	No	No	No
4	M	8	30	None	RT	25.6	None	33	Patchy	Yes*	0.9	1.2
5	M	11	37	None	RT and gemcitabine	31.2	None	39	No	No	No	No
6	F	13	44	Leptomeningeal and arachnoid metastases	RT and gemcitabine	34.7	None	32	Patchy	Yes	4.7	4.6
7	M	15	65	Tumor extension to nVII	RT and temozolomide	36.7	None	37	Ring	Yes	1.5	1.9
Total	57% M	11†	37†			31.5‡		34.1‡			2.7‡	3.1‡

*PET uptake was in area without gadolinium contrast enhancement.

†Median.

‡Mean.

RT = radiotherapy; nVII = facial nerve.

and 7.2 at 144 h after injection, respectively. In 1 patient, extension of the tumor in the facial nerve was seen on T2-weighted MRI, but there was no visually detectable PET signal.

Optimal Moment of Scanning and Dosimetry

There was no significant difference in the SUV_{mean} s for the 5 tumors with positive PET results at 72 and 144 h after injection (Fig. 2B). Because blood-pool activity declined over time, tumor-to-blood-pool SUV ratios were positively correlated with time after injection ($P = 0.045$) (Fig. 2C). Whole-body PET evaluation revealed that organ uptake of ⁸⁹Zr-bevacizumab among patients was, in contrast to that in tumors, quite homogeneous; uptake was highest in the liver and then in the kidneys, spleen, lungs, and vertebrae (Fig. 4). The mean effective dose per patient was 0.9 mSv/MBq (SD, 0.3 mSv/MBq) (Table 2).

DISCUSSION

There is an urgent need to predict the potential of a drug before therapy in children with brain tumors. In this first (to our knowledge) immuno-PET imaging study of pediatric oncology patients, we performed ⁸⁹Zr-bevacizumab PET imaging of children with DIPG and showed that the procedure is feasible without the use of anesthetics from the age of 6 y. We observed inter- and intratumoral heterogeneity of ⁸⁹Zr-bevacizumab uptake in 5 of 7 patients with DIPG, whereas the normal brain showed no uptake at all. Two of 7 primary tumors showed high-level but focal uptake, whereas ⁸⁹Zr-bevacizumab was not detectable at all in 2 DIPG tumors. The optimal time for scanning was 144 h after injection, as the tumor-to-blood-pool SUV ratios increased

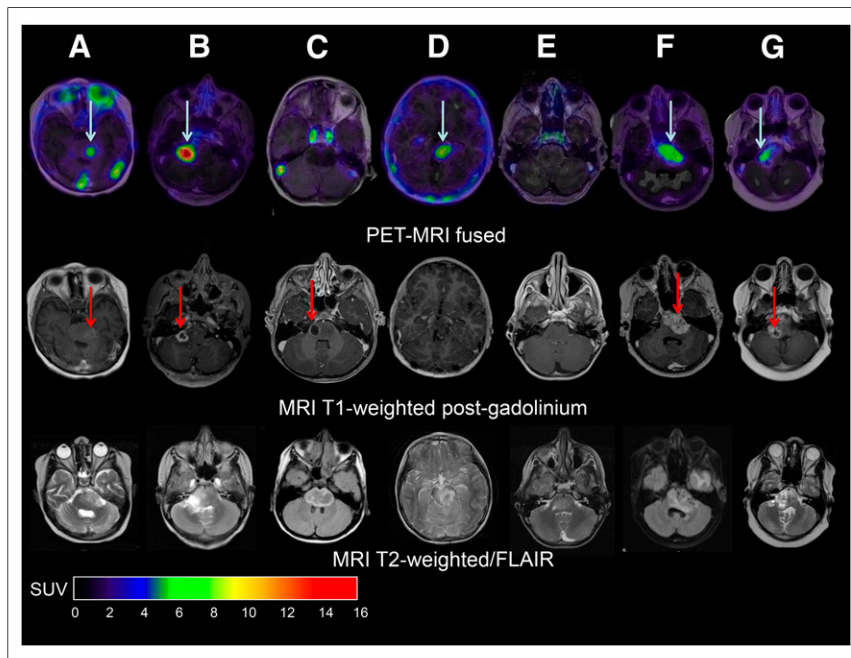


FIGURE 1. MR and PET/MR fusion images of patients with DIPG. (Top) ⁸⁹Zr-bevacizumab PET image (144 h after injection) fused with gadolinium-enhanced T1-weighted MRI image for each patient. (Middle) Gadolinium-enhanced T1-weighted MR images. (Bottom) T2-weighted/fluid-attenuated inversion recovery (FLAIR) MR images. Five tumors showed variable uptake of ⁸⁹Zr-bevacizumab (blue arrows), with areas within each tumor showing both negative and positive PET results. Two primary tumors (C and E) showed completely negative PET results, whereas T2-weighted images showed tumor infiltration in whole pons of both patients. Red arrows represent areas of contrast enhancement within tumor. In 4 of 5 primary tumors, areas showing positive PET results corresponded to contrast-enhanced areas on MRI (A, B, F, and G). Tumor in C showed MRI contrast-enhanced area but no ⁸⁹Zr-bevacizumab uptake. Tumor in D showed positive PET results but no gadolinium contrast enhancement on MRI.

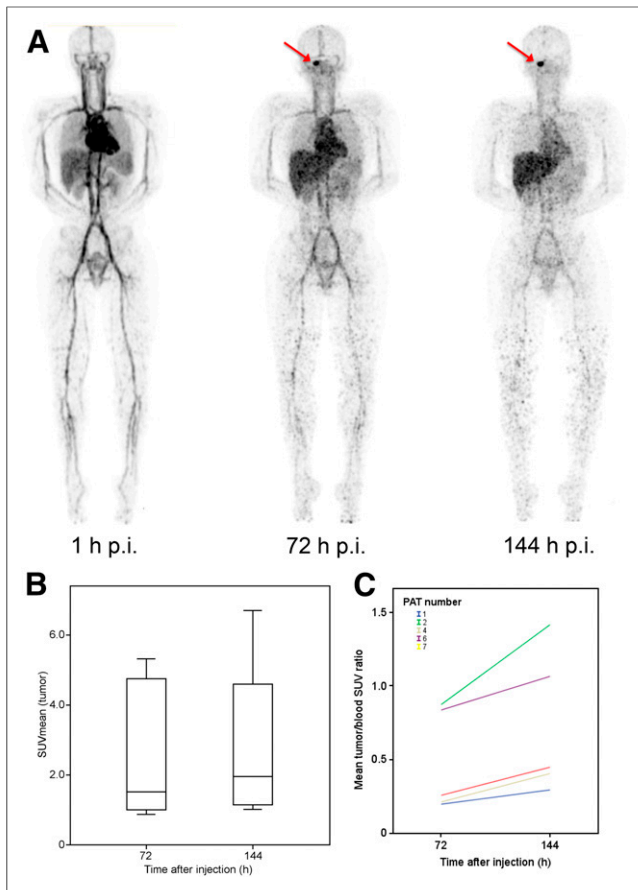


FIGURE 2. Correlation of tumor uptake of ^{89}Zr -bevacizumab with blood pool. (A) Whole-body PET images for 1 DIPG patient (patient 2) at 1, 72, and 144 h after injection. At 1 h after injection, maximum uptake was observed within blood pool. With increasing times after injection, blood-pool activity decreased significantly. There was no uptake of ^{89}Zr -bevacizumab in tumor at 1 h after injection, but there was clear uptake at both 72 and 144 h after injection (arrows). Uptake in liver was stable and represented vascularization (1 h after injection) and metabolism (72 and 144 h after injection) of ^{89}Zr -bevacizumab. p.i. = post-injection. (B) Box plots of tumor SUVs at 72 and 144 h after injection. SUVs were not significantly different ($P = 0.6$). (C) Tumor-to-blood-pool SUV ratios (measured in aortic arch) for each patient (PAT) as function of time after injection. SUV ratios were positively correlated with increasing times after injection (Kendall τ_b correlation coefficient, 0.524; $P = 0.045$; 2-tailed).

significantly over time. Therefore, we suggest the use of a single PET/CT scan at 144 h after injection in future studies.

The ^{89}Zr -bevacizumab uptake pattern in all tumors was focal; interestingly, 4 of 5 tumors showed significant ^{89}Zr -bevacizumab uptake only within MRI contrast-enhanced areas. Gadolinium uptake in the brain is associated with degradation of the blood-brain barrier; thus, when gadolinium-DPTA, with an average molecular weight of 545 kDa, is able to pass the blood-brain barrier, other large molecules, such as bevacizumab (149 kDa), may be able to pass as well—although blood-brain barrier permeability is, of course, dependent on more than molecular weight alone. In addition, contrast-enhanced “leaky” tumors have been associated with a higher level of local VEGF expression (20). However, we observed high variability in the level of ^{89}Zr -bevacizumab uptake in gadolinium-enhanced areas (from intense to absent ^{89}Zr -bevacizumab

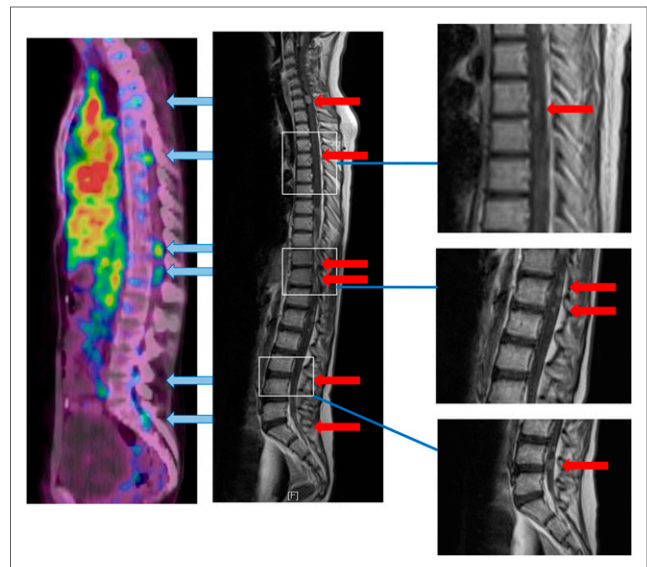


FIGURE 3. MR and PET/MR fusion images for 1 patient with primary DIPG and metastases in spinal cord. ^{89}Zr -bevacizumab PET/MR image in sagittal plane of spinal cord showed 6 ^{89}Zr -bevacizumab PET hot spots (left, arrows), which were all confirmed by gadolinium-enhanced T1-weighted MRI to be metastases (right, arrows). Some metastases were even clearer on PET than on MRI. All (11 in total) metastases showed positive PET results in this patient, whose primary tumor also showed high but focal ^{89}Zr -bevacizumab uptake (Fig. 1F).

uptake), suggesting large differences in local VEGF expression among DIPG tumors. Moreover, 1 tumor showed ^{89}Zr -bevacizumab uptake in an area without gadolinium contrast enhancement. Unfortunately, we were not able to validate VEGF expression in tissue,

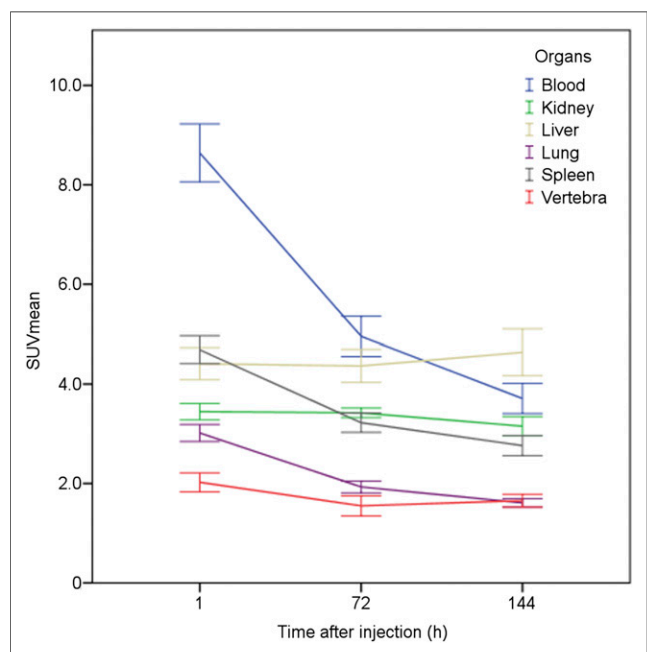


FIGURE 4. SUVs of normal organs. Data represent correlation of SUV_{mean} s with time after injection (error bars = 1 SD). ^{89}Zr -bevacizumab uptake in organs was constant among patients, in contrast to that in tumors.

TABLE 2
Absorbed Dose and Effective Dose for Individual Subjects

Patient	Absorbed dose (mGy/MBq)							MIRD age (y)	Sex	Effective dose (mSv/MBq)
	WB ROI	Kidneys	Liver	Lungs	Spleen	Bone marrow	RoB			
1	94.3	1.8	12.9	6.5	0.8	2.1	70.3	5	F	1.37
2	77.7	1.5	12.6	9.1	1.4	4.5	48.6	15	F	0.57
3	97.9	1.2	10.5	7.9	0.6	2.8	74.8	5	M	1.43
4	98.2	1.7	11.1	7.5	0.9	2.9	74.1	10	M	0.93
5	107.0	1.3	11.0	7.7	0.8	2.9	83.3	10	M	0.99
6	115.2	1.9	13.2	8.0	1.1	3.5	87.6	15	F	0.73
7	109.3	2.0	8.5	6.2	4.1	2.7	85.7	15	M	0.73
Total (median)	98.2	1.7	11.1	7.7	0.9	2.9	74.8			0.9

WB = whole body; ROI = region of interest; RoB = remainder of body.

as biopsies are not done routinely in DIPG patients. At least the clear differences in SUVs among gadolinium-enhanced tumors (reflecting differences in local drug uptake) and the presence of drug uptake in tumor areas without gadolinium contrast enhancement suggested that MRI alone is insufficient to predict the tumor accumulation of large molecules such as bevacizumab and that immuno-PET is of additional value.

We realize that the influence of radiotherapy is important. In our preclinical study with nonirradiated DIPG mouse models, we observed poor uptake of ⁸⁹Zr-bevacizumab in intracranial tumors (7). In the present study, the fact that the patients had completed radiotherapy at least 2 wk earlier may have induced a temporary disruption of the blood–brain barrier as well as increased VEGF expression via the mitogen-activated protein kinase pathway (21). We expected that DIPG patients would be more eligible for bevacizumab treatment after radiotherapy and that the effect on blood–brain barrier integrity would dissipate with increasing time after radiotherapy. Therefore, ideally, scans should be performed before, during, and after radiotherapy in each patient to determine the susceptibility of tumors to bevacizumab over time.

More studies are needed to show the correlation of tumor uptake of ⁸⁹Zr-bevacizumab and the response to treatment in DIPG patients. In adults with renal cell carcinoma, it has been shown that a high level of baseline ⁸⁹Zr-bevacizumab uptake in tumors before treatment is positively associated with time to progression in bevacizumab-treated patients (13). A difficulty in performing such a study with DIPG patients is that current DIPG trials involve multiagent therapy regimens. The finding that bevacizumab can reduce the penetration of other drugs into tumors (22,23) underlines the need for labeled-drug imaging in this multiagent setting. On the other hand, in contrast to single-agent settings, multiagent therapy may confound the association of the imaging biomarker and outcome—so that clinical validation of this immuno-PET method as a predictive biomarker of the response to therapy requires larger datasets. However, because immuno-PET allows for international application (long physical half-life of ⁸⁹Zr; relatively simple, centrally or locally performed radiochemistry), we suggest (on the basis of the data from the present pilot study) the inclusion of this method in future international DIPG clinical trials. Furthermore, molecular

imaging data from different trials could be included in the recently established SIOPE DIPG Registry to enable comparison of results.

Whole-body molecular drug imaging can help to predict organ-related toxicity. These data are particularly important in children because drugs developed to target overexpressed cancer-specific signal proteins (such as VEGF) also target tissues in which these proteins are expressed during children’s development. In the present study, the whole-body ⁸⁹Zr-bevacizumab biodistribution revealed a relatively high level of organ uptake in the liver and then in the blood, kidneys, lungs, and bone. These results are comparable to the results of the 2 ⁸⁹Zr-bevacizumab clinical trials in adults and correspond to the results of toxicity trials with bevacizumab in children; in these trials, hypertension, bleeding, elevation of the aspartate aminotransferase level, and proteinuria were reported as the main side effects (13,14,24). We observed moderate bone uptake, but osteonecrosis is a rarely reported symptom in bevacizumab-treated children (1%). Whether ⁸⁹Zr-bevacizumab uptake also correlates with long-term organ or bone toxicity needs to be addressed in long-term follow-up studies of children treated with bevacizumab.

The mean effective dose in the present study was slightly higher than doses of ⁸⁹Zr-labeled compounds in studies with adults (25); this finding likely was due to the age-dependent weight factors in the dosimetry models. In the present study, the 29-mSv radiation burden of immuno-PET (including 3 low-dose total-body CT scans) for an average DIPG patient (25 kg) was considerable, although in future studies the radiation dose will be reduced to 22 mSv because only 1 PET/CT (low-dose) scan of the brain will be performed. However, the possible benefits may outweigh the risks, especially in light of the poor prognosis (2-y survival of <10%) for patients with DIPG.

CONCLUSION

In the present study, we used immuno-PET imaging for pediatric cancer patients. The procedure was found to be safe and feasible in children without the use of anesthetics, and the optimal time for scanning was 144 h after injection. Clear differences in ⁸⁹Zr-bevacizumab uptake among DIPG tumors were observed, with 2 tumors showing no uptake at all. Interestingly, 4 of 5 tumors showed significant ⁸⁹Zr-bevacizumab uptake on PET within MRI

contrast-enhanced areas. However, we observed high variability in SUVs in these contrast-enhanced areas, suggesting differences in local VEGF expression, and we observed positive PET results in a non-gadolinium-enhanced area in 1 patient. Therefore, MRI alone seems to be insufficient for predicting drug accumulation in tumors. The results suggest that the addition of ^{89}Zr -bevacizumab PET imaging may be helpful in the selection of potential candidates for bevacizumab treatment of DIPG because this procedure assesses both target availability and drug accessibility of the tumor.

DISCLOSURE

This DIPG study was funded by the Semmy Foundation (Stichting Semmy) and the Egbers Foundation (Egbers Stichting). The Semmy Foundation and the Egbers Foundation, which fund DIPG research at VU University Medical Center, had no role in the study or preparation of this article. No other potential conflict of interest relevant to this article was reported.

REFERENCES

- Kaatsch P, Rickert CH, Kuhl J, Schuz J, Michaelis J. Population-based epidemiologic data on brain tumors in German children. *Cancer*. 2001;92:3155–3164.
- Hargrave D, Bartels U, Bouffet E. Diffuse brainstem glioma in children: critical review of clinical trials. *Lancet Oncol*. 2006;7:241–248.
- Jansen MH, Van Vuurden DG, Vandertop WP, Kaspers GJ. Diffuse intrinsic pontine gliomas: a systematic update on clinical trials and biology. *Cancer Treat Rev*. 2012;38:27–35.
- Jansen MH, Veldhuijzen van Zanten SE, Sanchez Aliaga E, et al. Survival prediction model of children with diffuse intrinsic pontine glioma based on clinical and radiological criteria. *Neuro Oncol*. 2015;17:160–166.
- Van Dongen GAMS, Huisman MC, Boellaard R, et al. ^{89}Zr -immuno-PET for imaging of long circulating drugs and disease targets: why, how and when to be applied? *Q J Nucl Med Mol Imaging*. 2015;59:18–38.
- Puget S, Philippe C, Bax DA, et al. Mesenchymal transition and PDGFRA amplification/mutation are key distinct oncogenic events in pediatric diffuse intrinsic pontine gliomas. *PLoS One*. 2012;7:e30313.
- Jansen MH, Lagerweij T, Sewing AC, et al. Bevacizumab targeting diffuse intrinsic pontine glioma: results of ^{89}Zr -bevacizumab PET imaging in brain tumor models. *Mol Cancer Ther*. 2016;15:2166–2174.
- Gururangan S, Chi SN, Young PT, et al. Lack of efficacy of bevacizumab plus irinotecan in children with recurrent malignant glioma and diffuse brainstem glioma: a Pediatric Brain Tumor Consortium study. *J Clin Oncol*. 2010;28:3069–3075.
- Hummel TR, Salloum R, Drissi R, et al. A pilot study of bevacizumab-based therapy in patients with newly diagnosed high-grade gliomas and diffuse intrinsic pontine gliomas. *J Neurooncol*. 2016;127:53–61.
- Zaky W, Wellner M, Brown RJ, et al. Treatment of children with diffuse intrinsic pontine gliomas with chemoradiotherapy followed by a combination of temozolomide, irinotecan, and bevacizumab. *Pediatr Hematol Oncol*. 2013;30:623–632.
- Aguilera DG, Mazewski C, Hayes L, et al. Prolonged survival after treatment of diffuse intrinsic pontine glioma with radiation, temozolamide, and bevacizumab: report of 2 cases. *J Pediatr Hematol Oncol*. 2013;35:e42–e46.
- van der Bilt AR, Terwisscha van Scheltinga AG, Timmer-Bosscha H, et al. Measurement of tumor VEGF-A levels with ^{89}Zr -bevacizumab PET as an early biomarker for the antiangiogenic effect of everolimus treatment in an ovarian cancer xenograft model. *Clin Cancer Res*. 2012;18:6306–6314.
- Oosting SF, Brouwers AH, Van Es SC, et al. ^{89}Zr -bevacizumab PET visualizes heterogeneous tracer accumulation in tumor lesions of renal cell carcinoma patients and differential effects of antiangiogenic treatment. *J Nucl Med*. 2015;56:63–69.
- Bahce I, Huisman MC, Verwer EE, et al. Pilot study of ^{89}Zr -bevacizumab positron emission tomography in patients with advanced non-small cell lung cancer. *EJNMMI Res*. 2014;4:35.
- Verel I, Visser GW, Boellaard R, Stigter-van Walsum M, Snow GB, van Dongen GA. ^{89}Zr immuno-PET: comprehensive procedures for the production of ^{89}Zr -labeled monoclonal antibodies. *J Nucl Med*. 2003;44:1271–1281.
- Cohen R, Stammes MA, de Roos IH, Stigter-van Walsum M, Visser GW, van Dongen GA. Inert coupling of IRDye800CW to monoclonal antibodies for clinical optical imaging of tumor targets. *EJNMMI Res*. 2011;1:31.
- Cohen R, Vugts DJ, Stigter-van Walsum M, Visser GWM, van Dongen GAMS. Inert coupling of IRDye800CW and zirconium-89 to monoclonal antibodies for single- or dual-mode fluorescence and PET imaging. *Nat Protoc*. 2013;8:1010–1018.
- Surti S, Kuhn A, Werner ME, Perkins AE, Kolthammer J, Karp JS. Performance of Philips Gemini TF PET/CT scanner with special consideration for its time-of-flight imaging capabilities. *J Nucl Med*. 2007;48:471–480.
- Stabin MG, Sparks RB, Crowe E. OLINDA/EXM: the second-generation personal computer software for internal dose assessment in nuclear medicine. *J Nucl Med*. 2005;46:1023–1027.
- Johansson M, Brannstrom T, Bergenheim AT, Henriksson R. Spatial expression of VEGF-A in human glioma. *J Neurooncol*. 2002;59:1–6.
- Park JS, Qiao L, Su ZZ, et al. Ionizing radiation modulates vascular endothelial growth factor (VEGF) expression through multiple mitogen activated protein kinase dependent pathways. *Oncogene*. 2001;20:3266–3280.
- Arjaans M, Oude Munnink TH, Oosting SF, et al. Bevacizumab-induced normalization of blood vessels in tumors hampers antibody uptake. *Cancer Res*. 2013;73:3347–3355.
- van der Veldt AA, Lubberink M, Mathijssen RH, et al. Toward prediction of efficacy of chemotherapy: a proof of concept study in lung cancer patients using [^{11}C]docetaxel and positron emission tomography. *Clin Cancer Res*. 2013;19:4163–4173.
- Fangusaro J, Gururangan S, Poussaint TY, et al. Bevacizumab (BVZ)-associated toxicities in children with recurrent central nervous system tumors treated with BVZ and irinotecan (CPT-11): a Pediatric Brain Tumor Consortium study (PBTC-022). *Cancer*. 2013;119:4180–4187.
- Börjesson PK, Jauw YW, Boellaard R, et al. Performance of immuno-positron emission tomography with zirconium-89-labeled chimeric monoclonal antibody U36 in the detection of lymph node metastases in head and neck cancer patients. *Clin Cancer Res*. 2006;12:2133–2140.